Ultrasonic Vibration-Assisted Keyholing Plasma Arc Welding

The interaction of ultrasonic vibration with the plasma arc results in improved heat-pressure features and the keyholing capability of the plasma arc

BY C. S. WU, C. Y. ZHAO, C. ZHANG, AND Y. F. LI

ABSTRACT

A process variant of plasma arc welding (PAW), i.e., ultrasonic vibration-assisted keyholing PAW process, was developed. The tungsten electrode connected with a specially designed ultrasonic transducer directly transmitted ultrasonic vibration into the plasma arc. The welding tests on stainless steel plates demonstrated that under the same conditions ultrasonic vibration can effectively improve the keyholing capability of the plasma arc so that an open keyhole can be produced with lower welding current and higher welding speed. The measurement results showed that the interaction of ultrasonic vibration with the plasma arc resulted in a further constriction of the arc column and a 15–31% increase in the plasma arc pressure under the conditions used in this study.

KEYWORDS

• Ultrasonic Vibration • Plasma Arc Welding (PAW) • Keyholing Capability
• Plasma Arc Pressure • Arc Constriction

Introduction

Nowdays because a variety of new high-performance materials are used in manufacturing, there is a big demand for advanced welding processes and equipment for joining medium-thick plates with high efficiency (Ref. 1). Plasma arc welding (PAW) is of application potential in joining medium-thick metal plates because it has advantages such as a big arc column stiffness, concentrated heat energy, large ratio of weld depth to width, and narrow heat-affected zone (Refs. 2–4). Compared to other high-density energy beam (laser and electron beam) welding processes, the PAW process and equipment are low in cost, easy in operation and maintenance, and strong in adaptability (Refs. 2, 5). However, conventional PAW still has some limitations, especially an insufficient keyholing capability for penetrating plate thickness as well as poor dynamic stability of the keyhole and weld pool (Ref. 6), which restrict the application of keyhole PAW.

To solve these problems, researchers recently developed some modified PAW processes. Vredeveldt designed and manufactured a new type of PAW torch, which added a cooling duct between the plasma gas and shielding gas ducts (Ref. 7). The gas inside the cooling duct flowed radially toward the root of the arc column at the torch bottom. Such added radial gas flow was supplied through a porous ring so that the radial diameter of the plasma arc was further reduced at the orifice exit. In this way, the heat density of the plasma arc was increased by the additional radial gas flow.

Mahrle et al. developed a laser-assisted PAW process, where the commonly solid tungsten electrode was replaced by a hollow one with an internal diameter of 1.2 mm, and a low-power laser was projected through the hollow tungsten electrode and passed through the plasma arc (Ref. 8). The laser interacted with the plasma arc, the latter was enhanced and stabilized, and the welding speed was increased. However, such modifications required special design and fabrication of the plasma torch to integrate additional radial gas flow or laser beam, which increased the complexity of equipment and operations.

Zhang et al. proposed a quasi-keyhole strategy in PAW operating in a mode "one keyhole per pulse" (Ref. 9). For the current waveform with two declining substages, when the welding current changed from the peak level to the base level, the first substage was with a variable slope while the second one was with a fixed slope. Wu et al. developed a controlled pulse keyholing PAW process by employing a specially designed welding current waveform (Refs. 10–12). At the dropping stage of the welding current from the peak level to the base level, two substages of current decreasing with different slopes were added so that the sustainment and closure status of the keyhole were able to be actively controlled. But the increased number of the waveform parameters caused some difficulty of process optimization.

Ultrasonic vibration, as a kind of mechanical energy, has advantages of easy application and high energy usage efficiency (Refs. 13, 14). Sun et al. used ultrasonic energy in gas tungsten arc welding (GTAW) (Refs. 15, 16). The GTAW torch was modified by including the ultrasonic transducer and the radiator. The tungsten electrode was inserted through the concentric hole of the ultrasonic radiator, and ul-

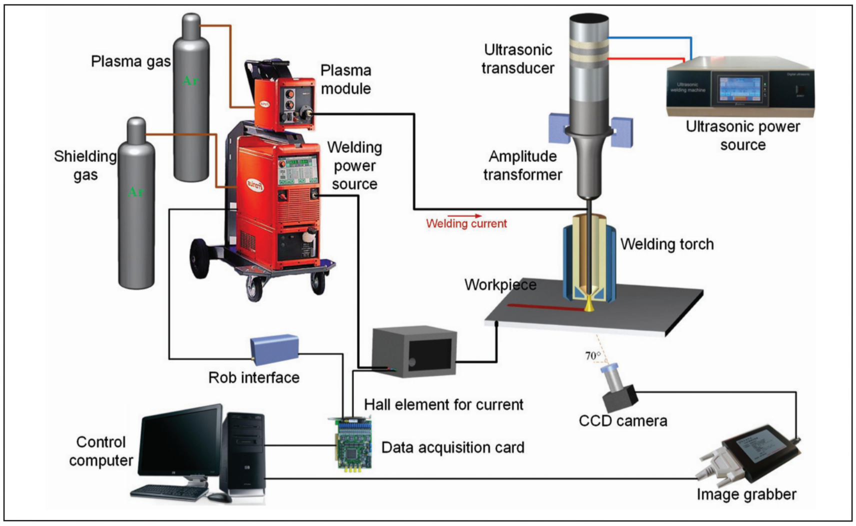

Fig. 1 — Schematic of ultrasonic vibration-assisted PAW system.

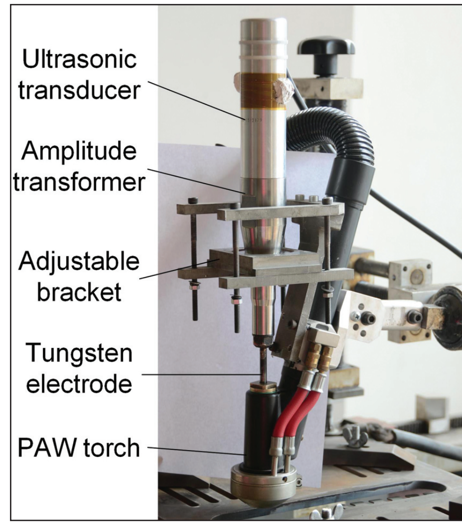

Fig. 2 — Photograph of ultrasonic vibration-assisted PAW torch.

trasonic vibration from the radiator was applied to the arc coaxially. The test results in welding of AISI Type 304 stainless steel showed that the ultrasound could significantly increase the weld penetration.

Fan et al. introduced ultrasound in gas metal arc welding (GMAW) to improve the metal transfer process (Refs. 17, 18). In their method, the main body of the welding torch was an ultrasonic vibration piezo-electric transducer and the filler material was fed through a concentric hole along its axis length. The ultrasonic wave was then radiated from the end of the ultrasonic radiator and reflected by the surface of the workpiece. This reflected wave interacted with the incident wave, thus forming an acoustic radiation field in the region of the arc column. With action of the ultrasound field, the gas metal arc was more contracted and became brighter, and its length was decreased. Under the same welding conditions, the presence of the ultrasonic field changed the globular transfer mode to the short-circuiting mode (Ref. 18).

For ultrasound-assisted GTAW and GMAW, the ultrasonic radiator with a much larger diameter than the tungsten/wire was used to transmit acoustic vibration into the arc column. It was found that the ultrasonic energy and the contraction degree of the arc are enhanced with the increase in the diameter of the ultrasonic radiator (Refs. 18, 19).

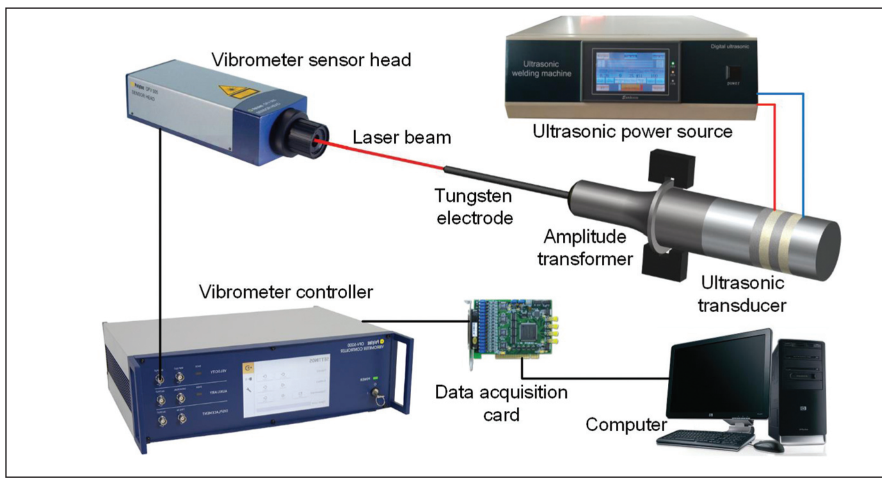

Fig. 3 — Measurement setup of ultrasonic vibration.

Because ultrasound-assisted GTAW and GMAW produced satisfactory process effectiveness, is it feasible to apply ultrasonic vibration in the PAW process to improve the keyholing capability of the plasma arc? For one thing, PAW has its own features. The PAW torch itself has a special structure, and the tungsten electrode is set back inside the torch (Refs. 2, 20). It is impossible to employ the ultrasonic radiator with a size larger than the diameter of tungsten/wire electrode, as in the cases of GTAW and GMAW. On the other hand, unlike gas tungsten arc and gas metal arc, the plasma arc itself has already been constricted by the orifice size (mechanical constriction) and the water-cooled nozzle (thermal constriction). Both mechanical and thermal constrictions greatly increase the current density in the plasma arc column. Thus, the electromagnetic constriction among the current lines inside the arc column is further enhanced, and the temperature and heat intensity are greatly improved (Refs. 2, 21). For the triple-constricted plasma arc with high heat intensity, is the additional ultrasonic vibration able to play a role in further improving the heat-pressure features and the keyholing capability of the plasma arc? It is a topic worthy of investigation.

In this study, a specially designed ultrasonic transducer was directly connected with the tungsten electrode, ultrasound was transmitted into the plasma arc via the electrode itself, and the ultrasonic vibration-assisted keyholing PAW system was developed. The welding tests on stainless steel plates were carried out to examine if

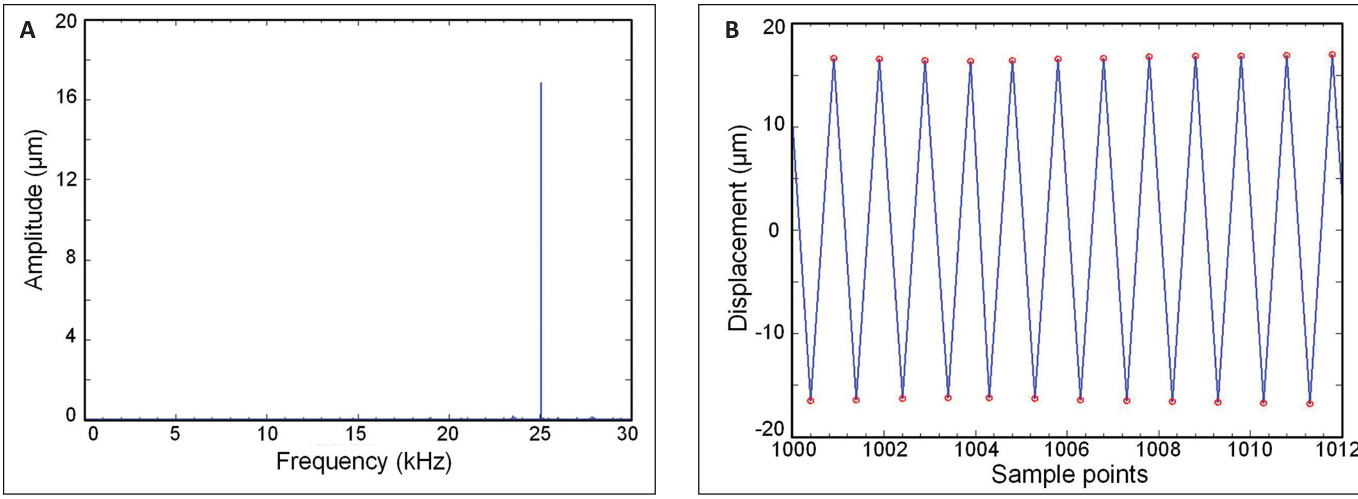

Fig. 4 — Measured results of the ultrasonic vibration system (200 W). A — Frequency and amplitude; B — section of processed waveform.

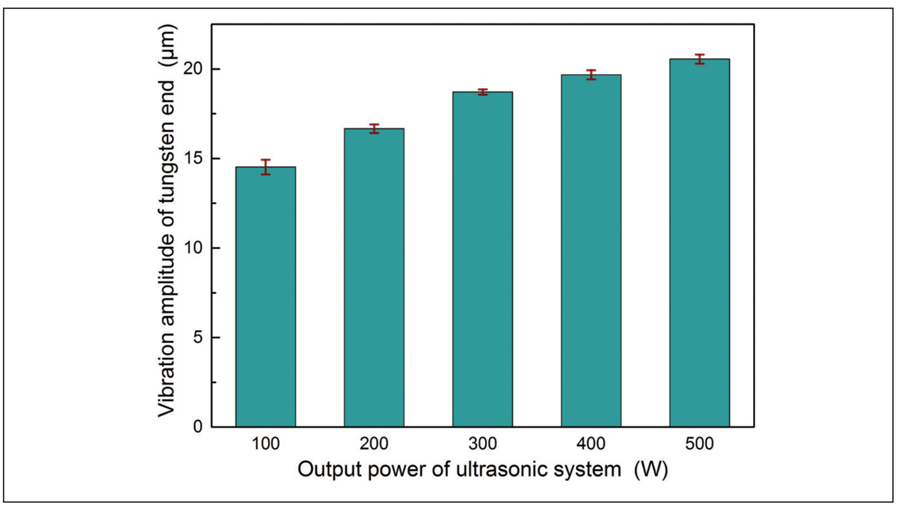

Fig. 5 — The vibration amplitude under different output powers of the ultrasonic system.

the additional ultrasonic vibration was able to play a positive role in improving the heat-pressure features and the keyholing capability of the plasma arc.

Experimental Setup

Experimental System

Figure 1 shows the schematic diagram of an ultrasonic vibration-assisted keyholing PAW system, which includes three main parts: the ultrasonic vibration unit, the plasma arc welding machine, and the sensing and control unit. The ultrasonic vibration system includes the ultrasound power source, the ultrasonic transducer, and the amplitude transformer. Under the electrical driving of the ultrasound power source, the ultrasonic transducer generated the ultrasonic wave that was amplified by the amplitude transformer and then transmitted to the tungsten electrode. The plasma arc welding system consisted of the digitally controlled TPS-5000 plasma generator and PTW-3500 plasma welding torch. During the welding process, the welding current and arc voltage were sampled via different sensing units in real time. Simultaneously, the keyhole exit at the underside of the workpiece was imaged by a CCD camera (OK-AM1101A) to determine if a keyhole channel that penetrated through the whole workpiece thickness was formed or not, as well as measured the keyhole behavior and dimension when such a fully penetrated keyhole is established. The CCD camera was equipped with a narrow band filter (with a central wavelength of 1060 nm, bandwidth of 20 nm, and transparency at 85%) and a neutral filter.

As shown in Fig. 1, the camera was aimed at the backside of the workpiece with an angle of 70 deg relative to the bottom surface of the workpiece. The captured image signals were digitized by the image grabber and processed by the control computer. During the welding process, the workpiece traveled at the welding speed, while the torch and the camera were stationary.

Figure 2 shows the assembly of the ultrasonic transducer, the amplitude transformer, the tungsten electrode, and the PAW torch. Because the end of the amplitude transformer was mechanically linked with the tungsten electrode, the latter vibrated axially with the same frequency as the ultrasound. The ultrasonic vibration from the tungsten electrode acted on the plasma arc, so that the latter's characteristics were changed.

Measurement of the Ultrasonic Vibration

When the ultrasonic system was manufactured and assembled, the measurement of the ultrasonic vibration at the end of the tungsten electrode was performed to determine if the vibration parameters met the design standard. To this end, a laser Doppler vibrometer (LDV) was employed to aim at the end of the tungsten electrode in a coaxial way, as shown in Fig. 3. The principle of the vibration measurement was as follows: The beam of a helium neon laser was pointed at the vibrating object and scattered back from it. The vibration amplitude and frequency were extracted from the Doppler shift of the reflected laser beam frequency due to the motion of the surface. The output of an LDV is generally a continuous analog voltage that is directly proportional to the target velocity component along the direction of the laser beam.

Figure 4 shows the measurement results. As designed, the electrode tungsten vibrated at a frequency of 25 (±0.5) kHz, and the vibration amplitude was about 17 μm under the power of 200 W — Fig. 4A. Figure 4B shows a section of the waveform captured from the processed wave. As the output power of the ultrasonic power source increased, the vibration amplitude of the tungsten electrode went up, as demonstrated in Fig. 5. The aim of this study was to employ a low but sufficient ultrasonic power to enhance the keyholing capability of the plasma arc. After some tests, it was found that the ultrasonic power source with 500 W output can provide enough acoustic influence on the plasma arc at a low cost.

Welding Test Conditions

As aforementioned, the CCD camera was employed to observe the keyhole exit from the backside of the workpiece. During the PAW process, the image of the keyhole exit was captured if an open keyhole was established. The welding tests were carried out on 304 stainless steel plates of 4 mm thickness. Both the plasma gas and the shielding gas were pure argon, and their flow rate was 2.6 and 20 L/min, respectively. The torch orifice was 3.2 mm diameter with a length of 3 mm. The tungsten electrode was 5 mm in diameter with a setback of 2 mm. The torch standoff was 5 mm. The output power of the ultrasonic system was 500 W. Other parameters are listed in Table 1.

Results

Keyhole Initiation and Stability

For Test Cases 1 and 2, the same welding current and welding speed were used, but the only difference was whether the ultrasonic vibration was exerted or not. Figure 6 shows the captured keyhole exit images for Test Cases 1 and 2. Under the same welding conditions, no open keyhole was established in conventional PAW without action of ultrasonic vibration, as shown in Fig. 6A. When the ultrasonic vibration was exerted, an open keyhole was formed so that the sequential images of the keyhole exit were observed — Fig. 6B. This means that ul-

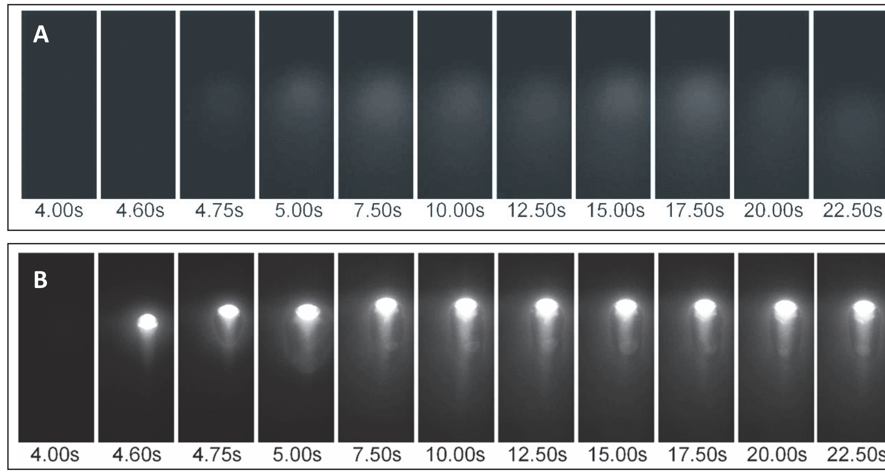

Fig. 6 — The captured keyhole exit images: A — Test Case 1, conventional PAW; B — Test Case 2, U-PAW.

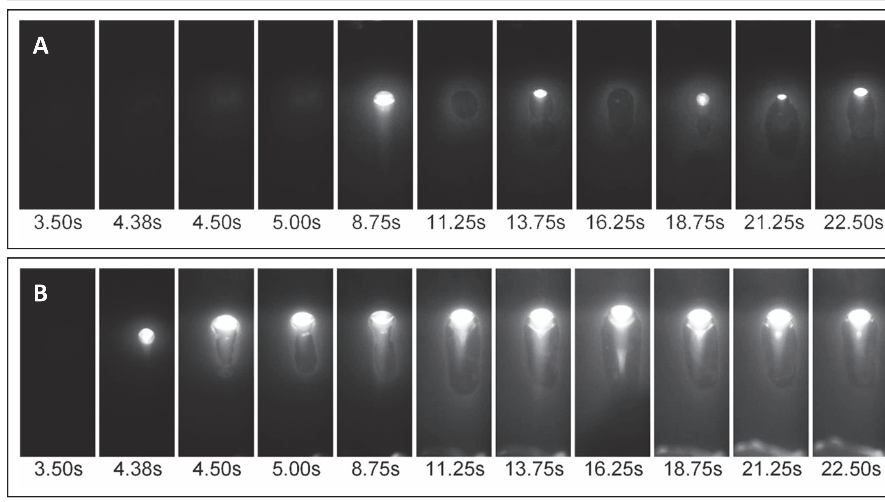

Fig. 7 — Stable open keyhole is established with lower welding current in U-PAW: A — Test Case 3, PAW, welding current 100 A; B — Test Case 4, U-PAW, welding current 90 A.

Table 1 — Welding Conditions

Test Case No.	Welding Current (A)	Welding Speed (mm/min)	Ultrasonic Vibration
1	80	100	No
2	80	100	Yes
3	100	110	No
4	90	110	Yes
5	95	100	No
6	95	115	Yes
7	110	120	No
8	110	120	Yes

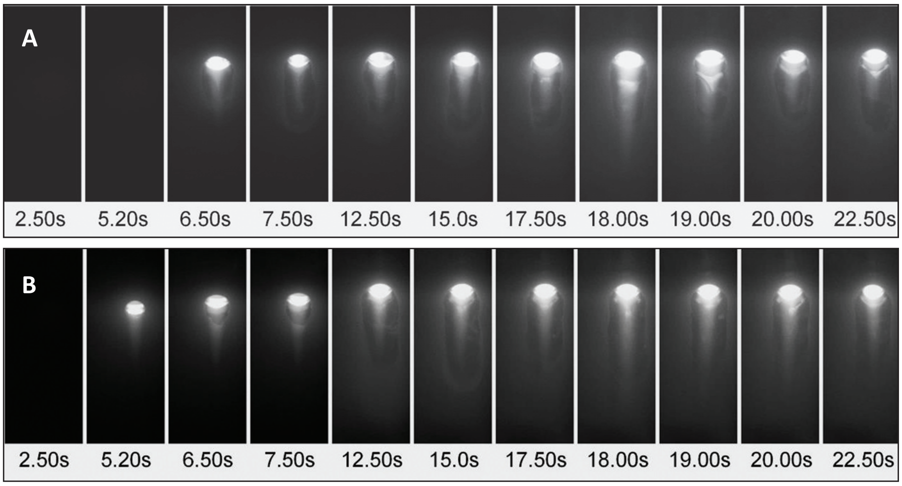

Fig. 8 — Stable open keyhole is established with higher welding speed in U-PAW: A — Test Case 5, PAW, welding speed 100 mm/min; B — Test Case 6, U-PAW, welding speed 115 mm/min.

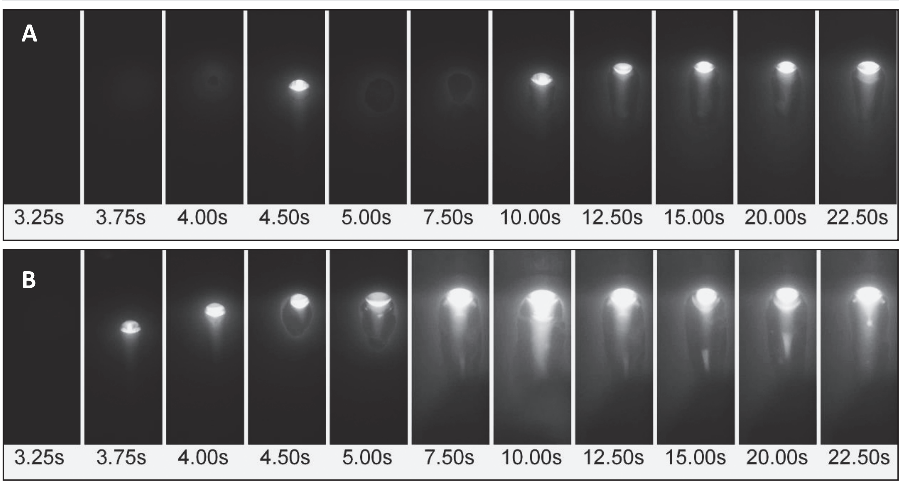

Fig. 9 — Comparison of keyhole exit images in PAW and U-PAW: A — Test Case 7, conventional PAW; B — Test Case 8, U-PAW.

trasonic vibration can enhance the keyholing capability of the plasma arc under the same welding conditions. During the ultrasonic vibration-assisted PAW (U-PAW) process, a penetrated keyhole was established first at instant t = 4.60 s, and the keyhole exit expanded its dimension until the moment t = 5 s. Then, the size of the keyhole exit remained the same, which means the quasi-steady state was achieved.

Because ultrasonic vibration can increase the keyholing capability of the plasma arc, a lower level of welding current may be used to get an open keyhole status and complete joint penetration in U-PAW if other welding conditions are the same. To validate this point, Test Cases 3 (PAW, welding current 100 A) and 4 (U-PAW, welding current 90 A) were made. For these two tests, the welding speed was 110 mm/min. In conventional PAW with a welding current of 100 A, an open keyhole was first established at instant t = 8.75 s, but it could not be maintained continuously because it was intermittently closed and opened — Fig. 7A. However, in U-PAW with a welding current of 90 A, an open keyhole was not only first established at instant t = 4.38 s, but it also kept a sustained open status once it was formed — Fig. 7B. It is obvious that under the same conditions, ultrasonic vibration can effectively improve the keyholing capability with reduced welding current but the weld penetration is guaranteed.

On the other hand, if the welding current is the same, a higher welding speed may be used in U-PAW. Test Cases 5 (PAW, welding speed 100 mm/min) and 6 (U-PAW, welding speed 115 mm/min) were performed. Under the welding current of 95 A, open keyhole was formed first at instant t = 6.50 s in conventional PAW with a welding speed of 100 mm/min — Fig. 8A. Whereas in U-PAW with a welding speed of 115 mm/min, an open keyhole was formed first at instant t = 5.20 s — Fig. 8B. Although a sustainable open keyhole was achieved in both test cases, U-PAW can run at a 15% higher welding speed than with PAW, and open keyhole was formed earlier. It is clear that ultrasonic vibration can enhance the keyholing capability through increasing the welding speed used under the same welding conditions.

With a little bit higher values of both welding current and welding speed, Test Cases 7 and 8 were further conducted to check out the effectiveness of ultrasonic vibration in enhancing the keyholing capability. As shown in Fig. 9A, the first open keyhole was formed at instant t = 4.50 s, but it was closed until instant t = 10 s in PAW. However, in U-PAW, the first open keyhole was formed at instant t = 3.75 s and it maintained the open keyhole status continuously — Fig. 9B. To compare the images in a quasi-steady state, i.e., the images within the period of 12.5–22.5 s in PAW and those within the period of 7.5–22.5 s in U-PAW, it can be seen that the size of the keyhole exit was larger in U-PAW than that of PAW. Under the same conditions, ultrasonic vibration can accelerate the establishment of an open keyhole, and make the established open keyhole reach quasi-steady state quickly.

Plasma Arc Pressure

As previously mentioned, exertion of ultrasonic vibration on the plasma arc can increase its keyholing capability. If the keyholing capability is enhanced, the pressure-heat features of the plasma arc must be improved by ultrasonic vibration. To examine this point, experiments were performed to measure the pressure distribution of the plasma arc.

The stagnation pressure measurement apparatus was used to detect the pressure of the plasma arc between a torch and an anode. The apparatus consisted of a water-cooled copper

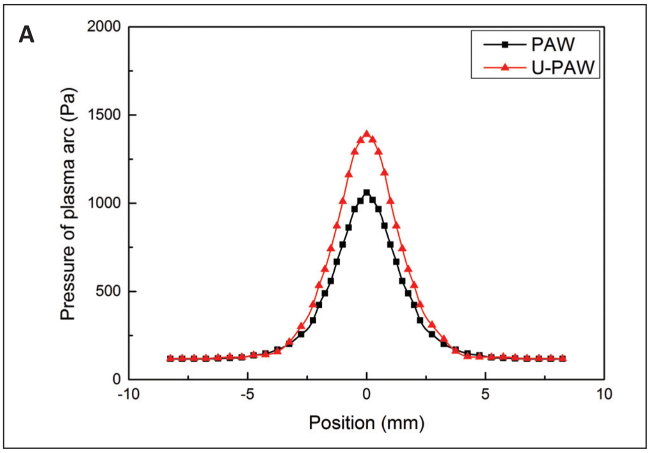

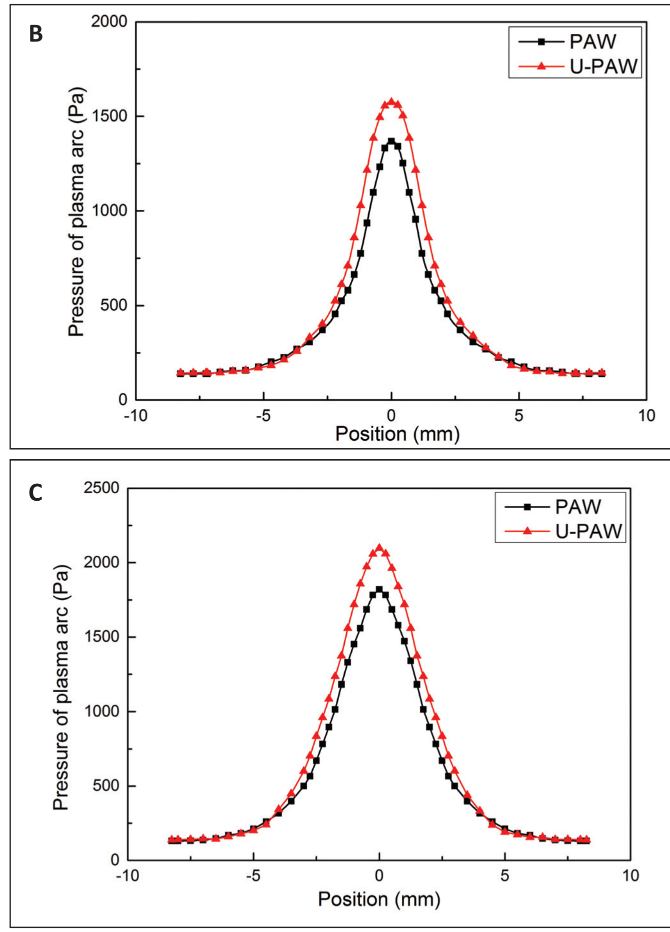

Fig. 10 — Plasma arc pressure distribution in PAW and U-PAW: A — 80 A; B — 100 A; C — 120 A.

block with dimensions of 140 mm length × 60 mm width × 22 mm thickness. The 0.5-mm-diameter measurement orifice was set in the copper block to lead the arc pressure into the sensor. At the bottom of the copper block, concentric to the measuring orifice with a short and thin pipe, a differential pressure sensor (PRC-905) with a measuring range of 0–5 kPa was assembled. A data acquisition card (PCI 8613) was set to sample the data during the test. At a position, the measurement was repeated ten times, and then the averaged value was obtained. During the test, the welding torch was stationary while the copper block was controlled via a precision three-dimensional slide platform, so that the relative movement between the welding torch and the sensor was obtained, and the distribution of the plasma arc pressure at different positions was obtained.

In this experiment, the plasma arc length, i.e., the distance between the nozzle end and the water-cooled copper block surface, was 5 mm. The ultrasonic power was set as 500 W, and the frequency of the ultrasonic system was 25 kHz. For this test case, both the plasma gas and the shielding gas were pure argon, and their flow rate was 2.6 and 20 L/min, respectively. The welding current took three levels of 80, 100, and 120 A.

Figure 10 compares the plasma arc pressure distribution in U-PAW (with ultrasonic vibration) and in conventional PAW (without ultrasonic vibration). With ultrasonic vibration, the arc pressure in U-PAW is always higher than that in conventional PAW. At the center of the anode corresponding to the plasma arc axis, the pressure difference between U-PAW and PAW was largest, and the gap between the two curves rapidly narrowed as the distance away from the center axis rose. For the peak value of the plasma arc pressure at the center axis, the difference between U-PAW and PAW became less when the welding current increased from 80 to 120 A. When the welding current was 80, the peak value of the plasma arc pressure was about 1390 and 1060 Pa for U-PAW and PAW, respectively, and the exertion of ultrasonic vibration made it increase by 31%. When the welding current was 120 A, the peak value of the plasma arc pressure was about 2098 and 1820 Pa for U-PAW and PAW, respectively, and the exertion of ultrasonic vibration made it increase by 15%.

Discussion

The test results in Figs. 6–9 demonstrated that U-PAW was able to achieve an open keyhole with a lower welding current or a higher welding speed under the same welding conditions. This implies that the interaction between the ultrasonic vibration and the plasma arc enhanced the keyholing capability of the plasma arc. The underlying mechanism may be explained as follows: A plasma arc is a mixture of three particles, i.e., atoms, electrons, and ions. The particles inside the plasma arc are driven to move at high speed by the electric field strength (potential gradient), the particle density gradient, and the temperature gradient (Ref. 22). When ultrasonic vibration is applied to a plasma arc, the particles are also exerted an extra force so that they vibrate too, as shown in Fig. 11. Such an extra vibration at high frequency is equivalent to the particle volume expanding along the vibration direction so that the contacting interface and the colliding probability of particles increase, which results in an increase of thermal conductivity of the plasma arc. The increment of thermal conductivity causes a forced cooling action to the plasma arc, which requires the plasma arc to generate more heat to compensate for this cooling effect. Thereby, the plasma arc has to automatically constrict its size at the transverse cross section to decrease its heat loss according to the

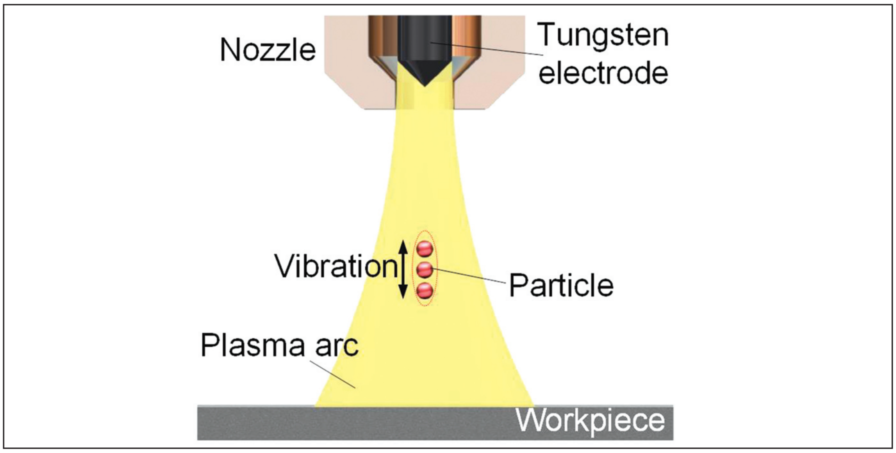

Fig. 11 — Schematic of particle vibration in U-PAW.

minimum voltage theorem in arc physics (Ref. 23). That means the ultrasonic vibration makes the plasma arc produce an extra constriction.

On the other hand, when ultrasonic vibration interacts with a plasma arc, the extra force exerted onto the particles will change the direction of the composite force on the particles. As shown in Fig. 12A, the electromagnetic force F_e and the plasma jet force F_p constitute a composite force F_{PAW} in the plasma arc. But for ultrasonic vibration-assisted plasma arc, the extra acoustic force F_u and the force F_{PAW} constituted a new composite force $F_{U\text{-}PAW}$, as demonstrated in Fig. 12B. The addition of F_u caused $F_{U\text{-}PAW}$ with a smaller angle with respect to the plasma arc axis so that the radial component of $F_{U\text{-}PAW}$ makes the plasma arc produce further constriction.

Due to the interaction between ultrasonic vibration and plasma arc, the two fold further radial constriction of the plasma arc gives rise to an increase in temperature, heat intensity, and flow velocity inside the plasma arc. Thus, the plasma arc pressure is increased, and the keyholing capability is enhanced.

The CCD camera was also employed to observe the plasma arc column generated between the torch and the water-cooled copper block. The captured raw images of the plasma arc were processed, and the plasma arc column beyond a certain gray value was extracted to characterize the main part of the plasma arc column with higher temperature and heat intensity. Figure 13 shows the extracted plasma arc column in PAW and U-PAW under the same conditions. It is clear that exertion of ultrasonic vibration made the plasma arc column be constricted under the same level of welding current. Such a constriction increased both the flow velocity of the plasma jet and the heat density inside the plasma arc. Therefore, ultrasonic vibration made the plasma arc have a higher pressure and heat density, which enhanced its keyholing capability.

The welding current has a predominant effect on the arc pressure and heat intensity. In fact, the arc pressure is directly proportional to the square of the welding current (Refs. 22, 23). When the welding current is low, the constriction extent of the plasma arc is not so high. Thus, there is room for further constriction by ultrasonic vibration. But the further constriction room becomes less when the welding current is higher because the welding current deduced constriction itself is already large enough. This is the reason why the increment of arc pressure due to ultrasonic vibration gets lower if the welding current is higher. The additional ultrasonic vibration can result in a 15–31% increase in the plasma arc pressure under the conditions in this study.

Conclusions

The following conclusions may be obtained:

1) The ultrasonic vibration-assisted keyholing PAW system was developed. A specially designed ultrasonic transducer was directly connected with the tungsten electrode, and ultrasound was transmitted into the plasma arc via the electrode itself.

2) The ultrasonic vibration can enhance the keyholing capability of the plasma arc. Under the same conditions, the additional ultrasonic vibration can produce an open keyhole with a lower welding current and a higher welding speed.

3) Compared to conventional PAW, the establishment of an open keyhole was accelerated and the quasi-steady state was reached in a shorter time in ultrasonic vibration-assisted PAW.

4) The additional ultrasonic vibration can result in a 15–31% increase in the plasma arc pressure under the conditions in this study. That is the reason why U-PAW has a strong keyholing capability.

5) The interaction of ultrasonic vibration with the plasma arc resulted in further constriction of the plasma arc column. However, the underlying mechanism needs further investigation.

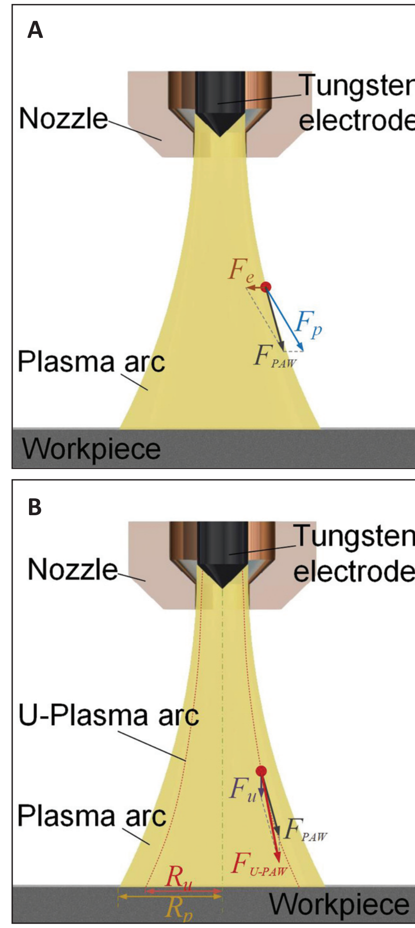

Fig. 12 — Comparison of the force acted on particles in the plasma arc: A — PAW; B — U-PAW.

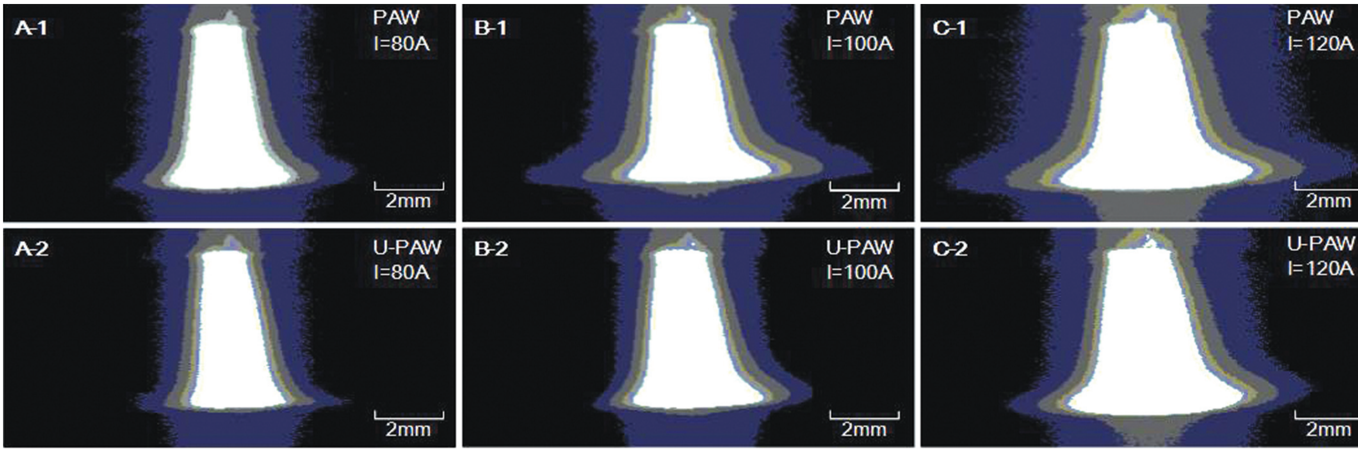

Fig. 13 — The dimensions of plasma arc column with/without ultrasonic vibration.

Acknowledgments

The authors are grateful for the financial support in this research from the National Natural Science Foundation of China under Grant No. 50936003.

References

1. Chinese Welding Society. 2016. *Welding Technology Roadmaps*. 121, Beijing, China Science and Technology Press.
2. Wu, C. S., Wang, L., Ren, W. J., and Zhang, X. Y. 2014. Plasma arc welding: Process, sensing, control and modeling. *Journal of Manufacturing Processes* 16(1): 74–78.
3. Gupta, M. R., Reddy, M. R., and Mukherjee, M. M. 2012. Key-hole plasma arc welding of 8 mm thick maraging steel — a comparison with multi-pass GTAW. *Welding in the World* 56(9–10): 69–75.
4. Martikainen, J., and Moisio, T. 1993. Investigation of the effect of welding parameters on weld quality of plasma arc keyhole welding of structural steels. *Welding Journal* 72(7): 329-s to 340-s.
5. Zhang, Y. M., Zhang, S. B., and Jiang, M. 2002. Keyhole double-sided arc welding process. *Welding Journal* 81(11): 248-s to 255-s.
6. Wu, C. S., and Jia, C. B. 2016. Plasma arc welding technology. In *Encyclopedia of Plasma Technology*, 1st Edition, DOI: 10.1081/E-EPLT-120053341, Taylor & Francis.
7. Vredeveldt, H. L. 2014. *Increased Power Density Plasma Arc Welding — The Effect of an Added Radial Gas Flow Around the Arc Root*. MS thesis. Delft, Netherland, Delft University of Technology.
8. Mahrle, A., Rose, S., Schnik, M., Beyer, E., and Fuessel, U. 2013. Stabilisation of plasma welding arcs by low power laser beams. *Science and Technology of Welding and Joining* 18(4): 323–328.
9. Zhang, Y. M., and Liu, Y. C. 2007. Control of dynamic keyhole welding process. *Automatica* 43: 876–884.
10. Wu, C. S., Jia, C. B., and Chen, M. A. 2010. A control system for keyhole plasma arc welding of stainless steel with medium thickness. *Welding Journal* 89(11): 225-s to 231-s.
11. Liu, Z. M., Liu, Y. K., Wu, C. S., and Luo, Z. 2015. Control of keyhole exit position in plasma arc welding process. *Welding Journal* 94(6): 196-s to 202-s.
12. Sun, J. H., Wu, C. S., and Feng, Y. H. 2011. Modeling the transient heat transfer for the controlled pulse key-holing process in plasma arc welding. *International Journal of Thermal Sciences* 50: 1664–1671.
13. Jose, M. J., Kumar, S. S., and Sharma, A. 2016. Vibration assisted welding processes and their influence on quality of welds. *Science and Technology of Welding and Joining* 21(4): 243–258.
14. Cunha, T. V., Enrique, C., and Bohorquez, E. N. 2015. Ultrasound in arc welding: A review. *Ultrasonics* 56: 201–209.
15. Sun, Q. J., Lin, S. B., Yang, C. L., and Zhao, G. Q. 2009. Penetration increase of AISI304 using ultrasonic assisted tungsten inert gas welding. *Science and Technology of Welding and Joining* 14(8): 765–767.
16. Sun, Q. J., Lin, S. B., Yang, C. L., and Zhao, G. Q. 2008. The arc characteristic of ultrasonic assisted TIG welding. *China Welding* 17(4): 52–57.
17. Fan, Y. Y., Yang, C. L., Lin, S. B., Fan, C. L., and Liu, W. G. 2012. Ultrasonic wave assisted GMAW. *Welding Journal* 91(3): 91-s to 99-s.
18. Fan, C. L., Yang, C. L., Lin, S. B., and Fan Y. Y. 2013. Arc characteristics of ultrasonic wave-assisted GMAW. *Welding Journal* 92(12): 375-s to 380-s.
19. Xie, W. F., Fan, C. L., Yang, C. L., and Lin, S. B. 2016. Effect of acoustic field parameters on arc acoustic binding during ultrasonic wave-assisted arc welding. *Ultrasonics Sonochemistry* 29: 476–484.
20. Shaw, C. B. Jr. 1980. Effect of orifice geometry in plasma-arc welding of Ti–6Al–4V. *Welding Journal* 59(4): 121-s to 125-s.
21. Li, X. G. 2007. Plasma arc welding and cutting. *Welding Handbook*, Vol. 1, 3rd Edition, Ed. by Chinese Welding Society, Beijing: China Machine Press, pp. 169–170.
22. Wu, C. S. 2011. *Welding Processes and Weld Pool Behaviors*. Boca Raton: Taylor & Francis/CRC Press, pp. 385–388.
23. Lancaster, J. F. 1986. *The Physics of Welding*. Oxford: Perganon Press, pp. 152–160.
24. Lin, M., and Eagar, T. W. 1986. Pressure produced by gas tungsten arcs. *Metallurgical Transactions B* 17(9): 601–607.
25. Oh, D. S., Kim, Y. S., and Cho, S. M. 2005. Derivation of current density distribution by arc pressure measurement in GTA welding. *Science and Technology of Welding and Joining* 10(4): 442–446.

CHUANSONG WU, Ph.D (wucs@sdu.edu.cn), *CHENG ZHANG, and YONGFENG LI are with the Institute of Materials Joining, Shandong University, Jinan, China. CHENYU ZHAO is with FAW-Volkswagen Automotive Co. LTP.*